








Cooling of gold cluster anions, Au_N^- ($N=2-13,15$), in a cryogenic ion-beam storage ring

Klavns Hansen ^{1,*}, Tian Weihao,² Emma K. Anderson,³ Mikael Björkhage,³ Henrik Cederquist ³, MingChao Ji ³,
Stefan Rosén,³ Alice Schmidt-May ³, Mark H. Stockett ³, Henning Zettergren ³,
Vitali Zhaunerchyk,⁴ and Henning T. Schmidt ³

¹Center for Joint Quantum Studies, Department of Physics, School of Science, Tianjin University, 92 Weijin Road, Tianjin 300072, China

²School of Science, Tianjin University, 92 Weijin Road, Tianjin 300072, China

³Department of Physics, Stockholm University, AlbaNova, SE-106 91 Stockholm, Sweden

⁴Department of Physics, University of Gothenburg, 41296 Gothenburg, Sweden



(Received 12 July 2024; accepted 29 October 2024; published 25 November 2024)

We measured the spontaneous and photoinduced decays of anionic gold clusters, Au_N^- , with sizes ranging from $N = 2$ to 13 and 15. After production in a sputter ion source, the size-selected clusters were stored in the cryogenic electrostatic ion-beam storage ring DESIREE, and their neutralization decays were measured for storage times between 0.1 and 100 s. The dimer was observed to decay by electron emission in parallel to neutral atom emission at long times, implying a breakdown of the Born-Oppenheimer approximation, analogous to the behavior of copper and silver dimers. Radiative cooling is observed for all other cluster sizes. The decays of clusters $N = 3, 6, 8-13, 15$ show only a single radiative cooling time. For $N = 6-13$ the cooling times have a strong odd-even oscillation with an amplitude that decrease with cluster size and with the even N having the faster cooling. We compare our results with previous measurements of radiative cooling rates of the corresponding cationic gold clusters, Au_N^+ , which also show an odd-even effect with a similar oscillation amplitude but at orders of magnitude shorter timescales and out of phase with the anions. The tetramer and pentamer both show two cooling times, which we tentatively ascribe to different structural forms at different ranges of high angular momenta of the ions in the Au_4^- and Au_5^- beams. For Au_7^- , the shape of the decay curve suggests that the cluster cools by emission of low-energy photons. The calculated limit on photon energies strongly suggests that cooling is by vibrational transitions in this case. For Au_5^- , time-resolved studies of photoinduced decays were performed to track the evolution of the internal energy distribution. We conclude that the radiative cooling is dominated by sequences of vibrational transitions in the IR. The laser-enhanced neutralization rate of Au_5^- was exponential, in contrast to its spontaneous decay rate, indicating that the cluster had already been cooled to a very narrow internal energy distribution at 120 ms as the total (integrated) laser-enhanced intensity was independent of the laser firing time at later times. The unimolecular rate constants decreased from 500 s^{-1} when laser excited at 0.12 s to 40 s^{-1} when laser excited at 0.62 s.

DOI: [10.1103/PhysRevA.110.052813](https://doi.org/10.1103/PhysRevA.110.052813)

I. INTRODUCTION

Quantization of electronic energies gives rise to a number of characteristic features of metal clusters. One of the strongest manifestations of these is odd-even effects, which were first observed for the intensity distribution as a function of size for small gold clusters by Katakuse *et al.* [1,2]. The gaps in the electronic excitation spectra associated with this effect and with shell structure decrease with increasing cluster size and ultimately give rise to thermally populated electronically excited states at some cluster size. This thermal excitation will cause a strong suppression of both the odd-even effect and the shell structure (see Ref. [3] for an analysis of the thermal suppression of the odd-even effect in gold clusters). It will also cause the appearance of the closely related effect of emission of electromagnetic radiation from

thermally populated electronically excited states, known as recurrent fluorescence (RF) [4] or Poincaré radiation [5,6].

The odd-even intensity effect is particularly strong for gold clusters, as judged by the abundances in the measured spectra of Katakuse *et al.* [1,2]. Also, the recurrent fluorescence is very strong for cationic gold clusters [7]. Intense RF was observed in experiments where cationic gold clusters were excited by laser light and unimolecular decays were measured in a time-of-flight mass spectrometer. RF implies the presence of low-energy optically active electronic states, and a spectroscopic experiment confirmed the presence of such absorption features for Au_{10}^+ [8] (cluster size 10 was the only one measured in that experiment). The radiative time constants observed in the experiments in Ref. [7] were very short for clusters up to size 9, on the order of microseconds, and showed a very strong odd-even oscillation, with radiative cooling times for even-electron-number (i.e., odd N) clusters typically an order of magnitude shorter than those for the odd-electron-number clusters and, for both types, orders of magnitude shorter than what can be explained by

*Contact author: KlavnsHansen@tju.edu.cn

infrared radiation from vibrational transitions. The correlation of radiative cooling timescales with electron number could potentially be ascribed to the higher per-atom excitation energy (effective temperature) for the even-electron-number (odd N) clusters. This was found not to be the case, however [9], and the main contribution to the strong even-electron radiative emission relative to the odd-electron clusters is therefore *not* due to their higher stability. Rather, the systematic is predominantly an intrinsic property associated with the number of valence electrons in some other way still to be understood. A similar conclusion was reached for the opposite question of whether the observed odd-even abundance oscillations are a radiative cooling effect. The analysis in [9] showed that also this is not the case. The radiative odd-even effect must therefore be considered an intrinsic phenomenon for cationic gold clusters.

In addition to the radiative cooling parameters for the gold cations, a number of other relevant parameters for the energetics of gas-phase gold clusters are known. They include ionization energies [10], electron affinities [11–13], and cationic dissociation energies [14,15]. Comparing the electron affinities in [12] and the atomic binding energies in [15], it is clear that the two types of binding energies tend to be of similar magnitude for a given size, with the reservations that the atomic binding energies pertain to cations and that the overlap in cluster size of the two studies is limited. The lowest activation energy channel determines whether electron emission or atomic evaporation dominates in statistical decays, modulo the effect of the different frequency factors for the loss of atoms and of electrons. The dominant channel sets the energy scale of the decaying clusters when decays occur from broad internal energy distributions. We therefore expect the effective temperatures of the present anionic clusters to be similar to those of the cations in the studies summarized in Ref. [7]. The question then naturally arises regarding whether the gold cluster anions will show RF and, if they do, whether they will show the same odd-even systematics as the cations.

Other questions arise as well. One is whether the effects of the high angular momenta inferred for some anionic copper [16] and silver clusters [17] are also present for gold clusters. The experimental signature is a decay rate which is a sum of two separate curves reflecting different angular momenta populations, each described by a power-law decay initially and modified by a radiatively generated exponential suppression at longer times.

A third question is whether the breakdown of the Born-Oppenheimer approximation recently seen for the anionic silver and copper dimers is also present for the gold dimer anion [18,19]. The breakdown was observed for the copper and silver dimers by detection of electron emission in competition with dissociation, which is the only possible decay channel within the Born-Oppenheimer description.

II. EXPERIMENTAL PROCEDURE

The clusters were produced in a cesium sputter ion source with currents of ~ 1 nA for the smallest species, decreasing with size to a fraction of a picoampere for $N = 15$. The clusters were accelerated to 10 keV ($N = 2-9$) or 5 keV

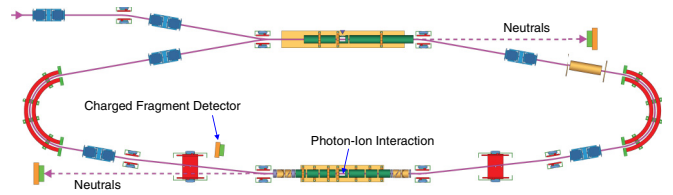


FIG. 1. Schematic of the ion-beam storage ring used for the present experiments on the spontaneous decay of Au_N^- clusters ($N = 2-13$ and 15) and of laser-induced decay of Au_5^- (see text).

($N = 10-13, 15$), limited by the maximum current in the mass-selection magnet.

Prior to injection into the ring, the mass spectrum of the ions produced in the source was measured by scanning the magnet. The spectrum showed a small but non-negligible presence of copper, which originated in the sputter source cathode. The combination of three atoms of the heavy copper isotope, of mass 65 u, is close enough to the mass of a single gold atom, 197 u, to potentially distort the decay curves by contamination.

The amount of such contamination was probed by a combination of two procedures. One was a comparison of the decay spectra recorded after mass selection centered at three different positions of nominal gold cluster peaks in the magnet scan: one on the low side, one at the maximum, and one on the high-mass side. The two spectra recorded with a setting on the maximum of the peak and on its high-mass side showed identical decay curves, indicative of a pure gold cluster sample. There was no sign of hydrides. In the other procedure, a cathode with a gold surface was used. A spectrum for the trimer showed a time dependence of the decay which was identical to that of the two high-mass curves in the previous test performed with the trimer. We concluded that these two magnet settings were sufficient to ensure beam purity. Since the beam current from the gold-surface cathode was not as stable as that from the standard cathode with a copper holder, the latter was used with the gold plug insert for most of the scans.

After mass selection, the cluster anions were injected into a single ring of the dual-ion-beam storage ring DESIREE [20,21], shown schematically in Fig. 1. The distance from the source to the midpoint of the side where the first fragmentation is detected (ℓ_s in the Appendix) is 6.4 m. The ions were injected from the top left, and neutral products from decays of all cluster sizes were detected at the right exit of the top section. The experiments with laser excitation applied an optical parametric oscillator (OPO) pulsed laser with pulse durations of around 5 ns and energies of typically 1 mJ. The light was unfocused. In the Au_5^- laser experiment, the laser beam crossed the ion beam in the middle of the bottom section, as indicated in Fig. 1, and the decay rate was measured with the lower left neutral detector. The dimer decay was measured with two detectors, viz., the detector in the upper right corner and the “fragment detector.” The top right detector counts all decays that produce a neutral particle and therefore gives the sum of the neutral atom emission and the electron detachment signal. The other one (“charged fragment detector”) detects only the fragments produced in the decay through the atom

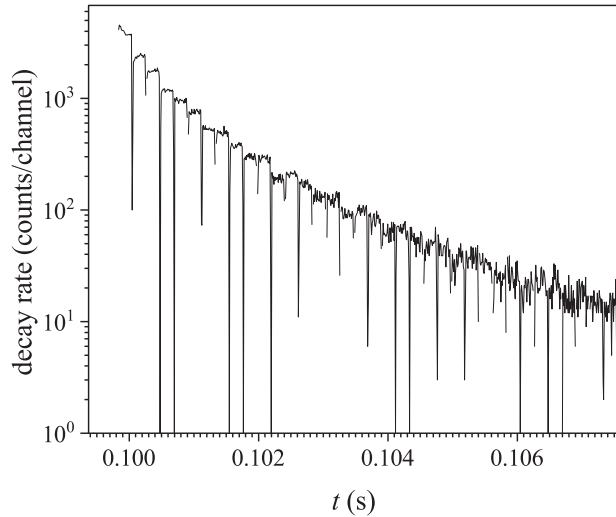


FIG. 2. The neutralization count rate of Au_7^- for the first 36 circulations in the ring, indicated by the plateaus of duration $\approx 200 \mu\text{s}$. The total storage time was 1 s. The time has not been corrected for the 100 ms used to record the background signal before ion injection. The unfilled 10% of the ring is seen as the dips in intensity.

emission channel. A comparison of the two detector signals showed the contribution from the electron emission channel. The arrangement is described in more detail in Refs. [18,19] for experiments on the copper and silver dimer anions.

Storage times varied between 100 ms and 100 s, depending on how fast the observed decay was quenched by the radiative cooling of the ions, if at all. The revolution times were $83\sqrt{N}\mu\text{s}$ for the 10-keV beams and, correspondingly, $\sqrt{2}$ longer for 5-keV ions. For most cluster sizes the ring was filled maximally, which is around 90%, but for a few of the highest beam currents, which were seen at the smaller cluster sizes, the ring was only partly filled to avoid detector saturation.

In Fig. 2 we show part of a raw-data spectrum for Au_7^- as an example of the measured spontaneous decay. In the analysis of the spectra, all counts for a turn in the ring were summed. Note that all decays in a specific turn can be assigned a single time after creation in the source. Summing over all decays in a single turn therefore does not introduce any approximations to the count rate vs time. Decay rates are therefore given as counts per turn in the ring. Counts may be binned over several turns with a bin size that increases proportionally with time to place the points equidistantly on a logarithmic-scale axis.

In addition to measurements of the spontaneous decay, the $N = 5$ clusters were exposed to laser light, and the photon-induced decays were measured. The laser system is EKSPLA NT 342 C, an optical parametric oscillator tunable-wavelength system. The light intersected the ions in a crossed-beam configuration (see Fig. 1). The laser repetition rate was 10 Hz, and the photon energy was 2.76 eV. For comparison the electron affinity is around 3.0 eV [22].

The data were recorded after the spontaneous decay of the hot clusters produced in the source was quenched by radiative cooling. The quenching was completed at the first laser firing time of 0.12 s. The laser light intensity was kept low enough to avoid depletion of the ion beam, and the neutralization ion

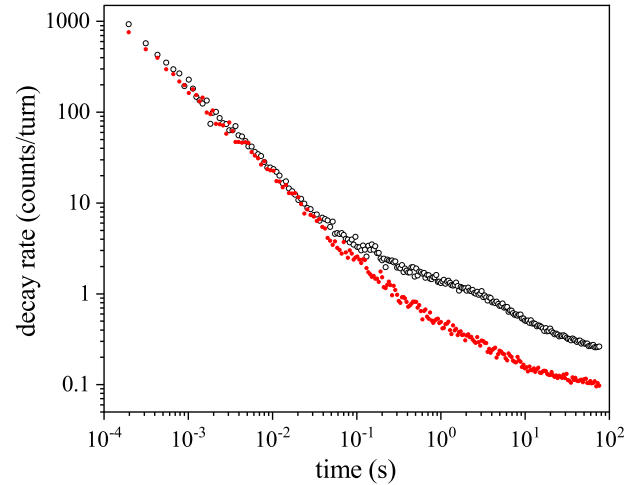


FIG. 3. The decay rate for the dimer anion vs time after the creation of the clusters in the source; the inclusive detector count is given by open black circles, and the fragment detector count is given by small solid red circles. The counts are bunched for statistics, as described in the text.

counts at different laser firing times can thus be compared directly.

The measured signal contains two background components besides the spontaneous or photoinduced neutralization count. One is generated by collisions with rest-gas molecules. This is a minor contribution due to the low temperature of the ring and the resulting very low pressure [21,23]. The main background contribution is the electronic noise from the detectors. To determine the detector dark count rate, the first 10% or 20% of each measurement cycle was recorded before the ions were injected. For the two neutrals detectors the dark count rates were around 5 s^{-1} in the experiment, similar to values seen previously in the same detectors. For the fragment detector it was somewhat higher but not prohibitively so.

III. RESULTS AND ANALYSIS

A. Decays of $N = 2$

In Fig. 3 we show the decay rate of the Au_2^- dimer for the all-inclusive neutral-particle detector on the upper right side of Fig. 1 and the fragment detector. The initial decay channel is completely dominated by the loss of a neutral monomer, as seen by the fact that the two curves coincide at early times. The initial decay rate follows a $1/t$ time dependence. This behavior is expected for decays from an ensemble of clusters with a broad distribution of rate constants [24]. For dimers with a single vibrational degree of freedom the decays are not thermally activated as in the description of typical unimolecular decays. Instead, the dominant decay at early times (dissociation) is due to tunneling out of the angular momentum barrier in the collection of the rotationally and vibrationally highly excited clusters created in the sputter source [25]. The power-law decay rate arises as a consequence of the broad distribution of tunneling rates for this process.

Around 30 ms, a difference between the two detector curves develops, indicating the appearance of a measurable contribution from the electron detachment channel, which soon after becomes dominant and remains so up to the end of storage at 80 s (see Fig. 3). The onset of a visible contribution from the electron emission channel coincides with a departure from the $1/t$ decay rate curve. The tunneling mechanism is not available for electron emission, which instead arises as a result of the breakdown of the Born-Oppenheimer approximation [18]. The breakdown is particularly striking for the coinage-metal dimers because the diabatic potential-energy curves of the anion and the neutral do not cross [11].

The behavior seen here for the gold dimer is almost identical to those of the copper and silver dimer anions [18,19], for which decays were measured up to 10 s. It remains an open question why the three coinage-metal dimer anions show such similarities for both the onset time of a visible contribution from electron emission and the electron-atom-emission branching ratio as a function of time.

B. Decays of $N = 3, 4, 5$

The decay rates of clusters Au_3^- , Au_4^- , and Au_5^- are, unlike those of the larger clusters, not well described by the combination of a single power law and radiative cooling parametrized with a single time constant [see Eq. (1) below]. The decay curves for these three clusters, shown in Fig. 4, are very similar to those seen for silver and copper anions of the same size (see Refs. [16,17]). A significant part of the analysis of the small silver and copper clusters applies to the three gold cluster anions with little change. Briefly, the source will produce gold clusters with a range of states with high rotational excitations. A distribution of angular momenta can give rise to two or a few different geometries of the clusters that are realized at different angular momenta, as discussed in detail in [16]. Conservation of angular momentum protects such conformers from free interconversion and causes the ions to decay as an ensemble of different species with different properties. Different geometric structures will, in general, have different radiative cooling rates; i.e., two or more radiation constants may be seen in the measured decay rate. We suggest that the presence of two such populations in the beam causes the structure in the decay rates of $N = 4, 5$, with their first relatively steep decrease followed by a slower decrease for the intermediate times between 10 and 100 ms. This behavior is most clearly seen for the tetramer ($N = 4$) but is also present in weaker form for the pentamer ($N = 5$). The suggestion is borne out by the fitted powers of the initial decay, which (numerically) exceed unity (-1.30 for $N = 5$ and -1.58 for $N = 4$) and are then understood as the residual of a radiative cooling component which has almost quenched at the beginning of the measurement time range of a few hundred microseconds. The values of the fitted powers reflect this initial cooling.

The trimer decay rate does not show the intermediate flattening of the decay curve. Another difference from the tetramer and pentamer is that the absolute value of the power on the initial decay is significantly below unity (see Table I). The only possible explanation we can give for this is that the trimer decays in a manner similar to the dimer by electron

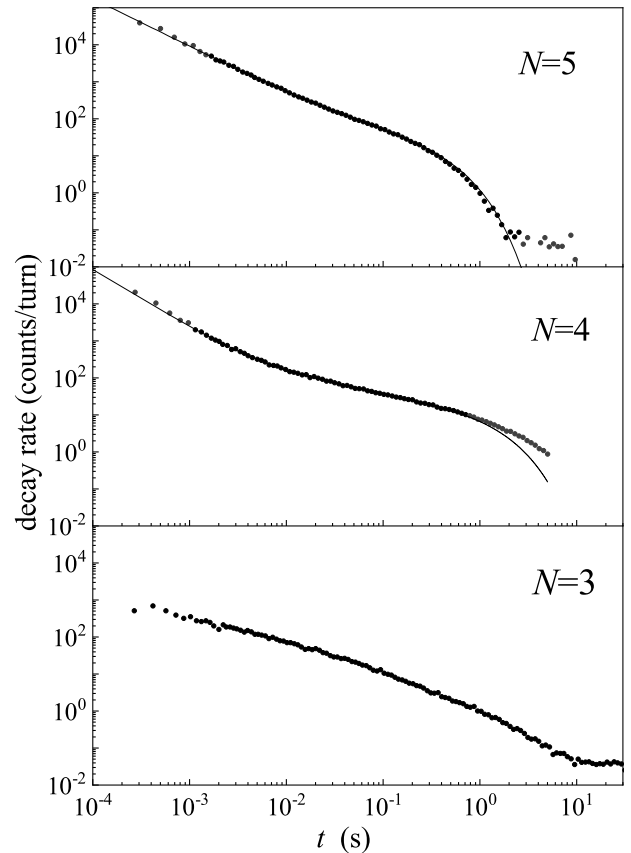


FIG. 4. The decay rates of clusters $N = 5, 4, 3$ (from top to bottom). The lines for the penta- and tetramer are the fitted curves, using a sum of two radiatively quenched decay rates. The trimer curve did not give a good fit. All spectra are measured with the all-inclusive neutral detector.

emission and, for similar reasons, up to ~ 10 ms, after which exponential quenching by radiative cooling sets in (the flat part of the spectrum after 10 s is background counts). To wit, the dimer decay rate flattens out at long times and appears to mimic a power-law decay with low power. Although the similarities are suggestive, the mechanisms behind this flattening are still unclear.

TABLE I. Powers and time constants as fitted with Eq. (1). The entries for $N = 7$ refer to fits at a relatively short time. Standard deviations of p and τ are given as σ_p and σ_τ , respectively.

N	p	σ_p	τ (ms)	σ_τ (ms)
3	0.79	0.01	2800	200
6	1.49	0.04	4.5	0.2
7	1.44	0.01	120	12
8	1.48	0.02	7.0	0.3
9	1.31	0.01	50	1
10	1.15	0.02	13.0	0.7
11	1.15	0.02	42	3
12	1.22	0.06	17	3
13	1.18	0.05	24	7
15	1.16	0.07	17	4

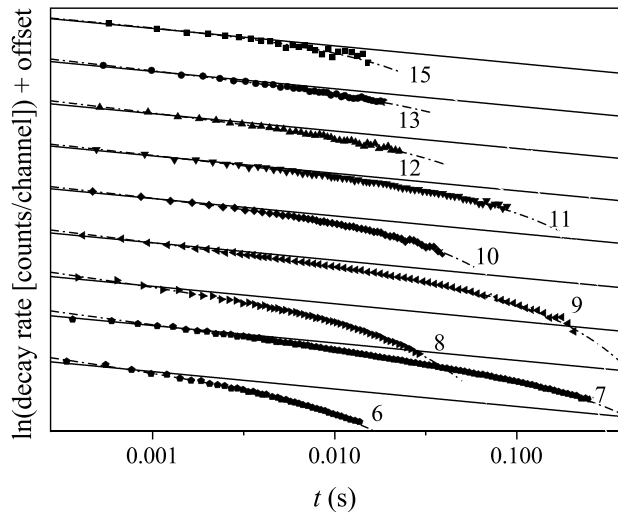


FIG. 5. The measured decay rates for clusters $N = 6-13, 15$ vs time t after the creation of the clusters in the source. The curves have been offset by a constant amount for display purposes. The ordinate scale is provided by the straight lines that are proportional to $1/t$.

C. Decays of $N = 6-13, 15$

In Fig. 5 we show the measured spontaneous decay curves for $N = 6-13, 15$. Like for the smaller clusters, the production of the clusters in the source leaves them highly excited at the time of injection into the ring. The curves are fitted with Eq. (1) [also $N = 7$; see below for a refit with Eq. (3)].

All sizes shown in Fig. 5 decay initially with close to the expected t^{-1} law rates, but with some powers in t^{-p} differing significantly from $p = 1$. A zoomed-in view of the initial decays is given in Fig. 6. The fitted powers are given in Table I.

At later times the decays quench and approach a quasi-exponential form for the decay rate. This is ascribed to radiative energy dissipation. An alternative suggestion is the freezing in of vibrational degrees of the product cluster, as seen for SF_6^- [26]. However, estimates of the level densities rule this out for the present study of gold cluster anions, and we will disregard this mechanism.

The radiative timescales are clearly dependent on cluster size, but also the fitted powers of the initial decay show some variation with size. In the simplest form the quenching of the neutralization rate is described by the exponential factor in the expression

$$R \propto t^{-p} e^{-k_r t} \equiv t^{-p} e^{-t/\tau}. \quad (1)$$

This equation pertains to the emission of large energy photons with rate constants k_r , large energy in the sense that the emission of a single photon quenches any further unimolecular decay. Equation (1) is the expression used for the fits for most cluster sizes here. The alternative expression, given below, describes the time constant for photon energies that are so small that their effect must be described as continuous cooling of the cluster. The spontaneous decay of Au_7^- is described better by that form. A thorough discussion of the area of applicability of the large and small photon energy quenchantings is given in Ref. [27]. We show in Table I the powers p and time constants τ from fits with Eq. (1), including a fit for the heptamer for

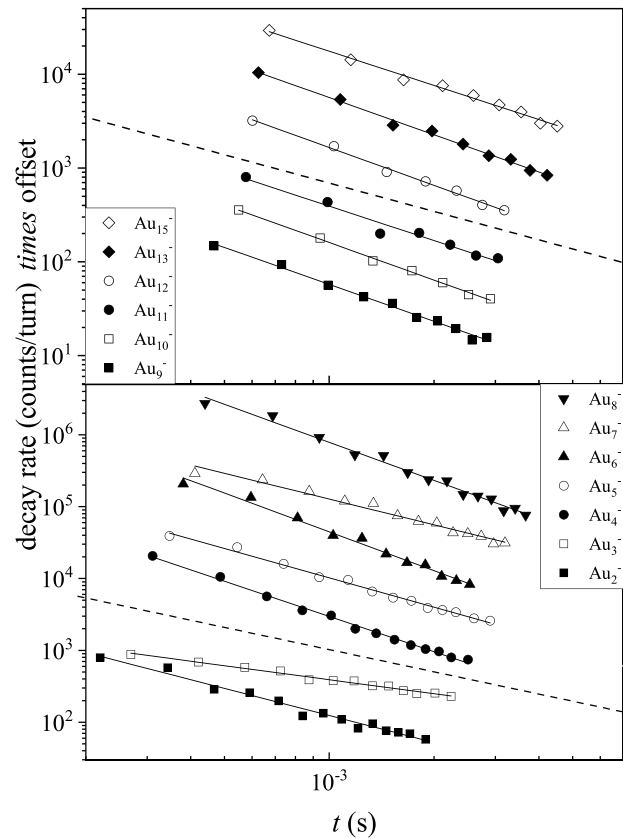


FIG. 6. Fits of the initial decay rates for all clusters Au_N^- , $N = 2-13, 15$. The dashed line is the $1/t$ decay multiplied by an arbitrary constant.

a relatively short time range. In Fig. 7 we show the fitted values of p for $N \geq 6$. There is a clear deviation from a unit power, $p = 1$, which decreases with size and reaches a value a little above unity for the larger cluster sizes. The value of

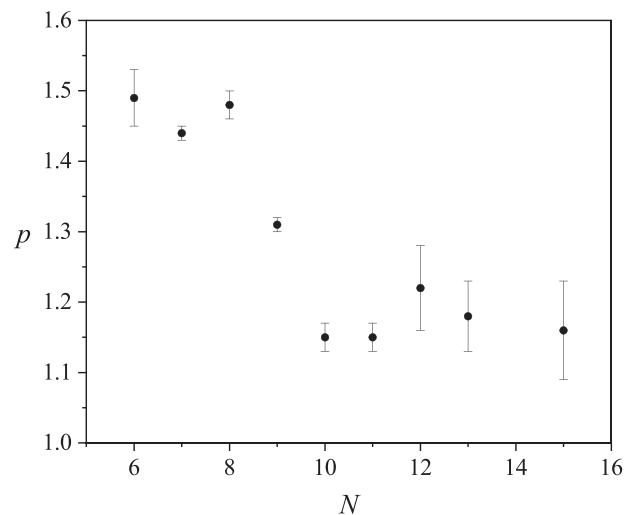


FIG. 7. The fitted values of the power in the initial power-law decay p , listed in Table I. The decays were single component curves for the clusters shown, $N = 6-13, 15$. The error bars give the one-standard-deviation fitted values.

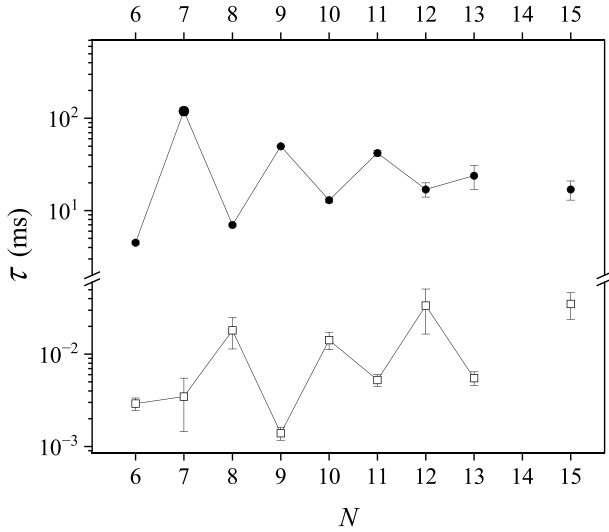


FIG. 8. The radiative cooling constants measured here for the gold anion clusters $N = 6$ –13, 15 (solid circles). The open squares show the time constants for cationic gold clusters (the values are slightly shifted from the values in [7] due to the inclusion of an additional data set).

p is expected to deviate slightly from unity, mainly due to the effect of the finite heat capacity of the clusters. The expression is [28]

$$p = 1 + \delta + 2\delta \frac{e^{-\delta \ln \omega t}}{1 - e^{-\delta \ln(\omega t)}}, \quad (2)$$

with $\delta \equiv 1/(C_v/k_B - 1)$, where C_v is the canonical (vibrational) heat capacity, t is the observation time, and ω is the frequency factor of the observed unimolecular decay, thermionic emission, or atomic evaporation, whichever the case may be. The expression reduces to $p \approx 1 + 2/\ln(\omega t)$ for large heat capacities. The calculated values for clusters $N = 10$ –15 are 1.08 to 1.09 for $\ln(\omega t) = 25$ and an effective heat capacity of $(3N - 7)k_B$, corresponding to thermionic emission from harmonic oscillator clusters ($3N - 7$ is the relevant value for a microcanonical ensemble of harmonic oscillators; see [29]). The observed values for $N \geq 10$ are a little higher than this estimate but not unreasonably so, considering that the heat capacities are not precisely known. For the smaller clusters, $N = 6$ –9, the observed values of 1.3 to 1.5 are too large to be explained in that way.

The explanation for the high values that we find most plausible is that the measured power is masking the residual of a radiative cooling component which occurs during transit from the source to the ring. This explanation requires the co-existence of isomer populations in the beam, similar to those inferred previously for rotationally highly excited species for the copper and silver anion clusters [16,17] and as discussed above for Au_4^- and Au_5^- . Further experiments are required to clarify the picture.

In Fig. 8 we show the radiative cooling time constant τ for Au_N^- , $N \geq 6$, as solid circles. The data show a striking odd-even effect similar in magnitude to that of the *cations*, although with two important differences. One is that the time constants are 3 to 4 orders of magnitude larger than those for

the cations [7], shown as open circles. The other difference is that the effect has opposite phases for anions and cations.

The presence of the odd-even effect in the radiative cooling of the anions has features that give conflicting indications of its origin. On the one hand, the bare existence of odd-even oscillations as a function of the number of electrons indicates an electronic origin, similar to the odd-even effect in abundances and in the (cationic) cluster binding energies. The electron spin degeneracy of single electrons summarizes this oscillating behavior. The odd-even staggering is then the result of electronic structure. With respect to radiative cooling, this indicates RF emission, at least for the even- N clusters. Likewise, the similar amplitudes in the size-to-size oscillations for anions and cations suggests an electronic origin of the cooling. Such variations in oscillator strengths in vibrational emission are not seen in other systems to our knowledge.

On the other hand, the average emission rates are rather small for RF radiation. Furthermore, the periodicity has, as noted, the phase opposite to the cationic case. This is not expected for electronic transitions because the difference in the charge state of cations and anions is 2, corresponding to a full period of the oscillations.

We will tentatively conclude that the radiation involves vibrational cooling in some form, although contributions from electronic transitions cannot be excluded. One possibility is that the odd-electron species have access to low-lying electronic excitations that are absent for even-electron clusters.

D. $N = 7$

The fitted values for the power and radiative cooling constant for clusters $N = 7$ that are given in Table I refer to relatively short times after production in the source. Including longer times yielded systematically different parameters of the fit function $t^{-p} \exp(-t/\tau)$. To understand this better we will analyze the decay of this cluster in more detail. One step is to consider the expression for cooling through the emission of photons with small energies, for which the neutralization rate becomes [27]

$$R \propto 1/[\exp(t/\tau) - 1]. \quad (3)$$

This expression describes the situation where the clusters retain enough energy to decay even after emission of one or several photons. It is derived by an expansion of the logarithm of the rate constant k with respect to energy and by assuming that the emitted power, $-dE/dt$, is time independent [27,30]:

$$1/\tau = \frac{d \ln k}{dE} \left(-\frac{dE}{dt} \right). \quad (4)$$

A simple derivation of the expression in Eq. (3) is found in Ref. [27]. For completeness we reproduce the calculation here: With a constant emitted power, the rate constant for a cluster of initial energy E varies to first order in time approximately as

$$k(E, t) = k(E, 0)e^{-wt}, \quad (5)$$

with

$$w \equiv -\frac{d \ln k}{dt}. \quad (6)$$

The derivative is taken at zero time at the energy E that corresponds to the one for which the rate constant is equal to the reciprocal radiation time, $k(E) = 1/w$, similar to the procedure used in Ref. [31]. The exponential arises because of the strong variation of k with energy and does not require any other feature of the energy dependence. Calculating the observable total decay rate $R(t)$ with due consideration to the depletion prior to t gives

$$R(t) \propto \int_0^\infty g(E) \exp\left(-\frac{k(E, 0)}{w}(1 - e^{-wt})\right) k(E, 0) e^{-wt} dE, \quad (7)$$

where $g(E)$ is the initial distribution of excitation energies E of the clusters. Up to multiplicative factors that are time independent to a good approximation, the time dependence of this integral is identical to the one that gives the non-radiative power-law decay after the substitution $t \rightarrow [1 - \exp(-wt)]/w$. In applications it should be noted that the expression is derived with a first-order expansion, and it will therefore not cover decays at all times, but it is a decent approximation and differs in an observable manner from the large photon energy limit of Eq. (1).

In order not to bias the fit, an expression for the parallel emission of both small and large photons is used:

$$R \propto t^{-p'} \frac{\exp(-t/\tau_1)}{\exp(t/\tau_2) - 1}. \quad (8)$$

Although the fit will show that τ_1 is effectively infinite, i.e., that there is an unobservable amount of large photon energy cooling, clearly the full expression [Eq. (8)] is required to show this. We also find it useful to include it for future reference. The value of p' is the correction to the $p = 1$ power law for nonideal behavior, i.e., $p' = p - 1$, as can be seen if the exponential in the denominator is expanded for times short relative to τ_2 . The interpretation of Eq. (8) is interesting. The equation expresses the two reasons the neutralization decays can be suppressed by radiative cooling: One is the factor giving the large photon suppression, $\exp(-t/\tau_1)$. This has the effect that the *population* of the decaying particles decays exponentially, or, more correctly, is converted into clusters with energies that are so low that the ions will remain intact. The other factor, due to the emission of small energy photons, $1/[\exp(t/\tau_2) - 1]$, causes instead the unimolecular *rate constants* to decrease exponentially. See Ref. [27] for details and Ref. [32] for an example of parallel large and small photon energy radiative channels for C_{60}^- .

In Fig. 9 we show a fit of the decay curve with the modified general cooling rate expression in Eq. (8). The curve is best fit with $p' = 0.35$, $\tau_2 = 60$ ms, and $\tau_1 = \infty$, compared to the values $p' = 0.44$ and $\tau_1 = 120$ ms from the fit to Eq. (1), where τ_2 was constrained to be infinite instead.

With some assumptions, the value of τ_2 can be used to find the emitted power. The rate constant k describing the electron emission of a cluster with electron affinity A_e and a level density of $(E + E_0)^{s-1}$ is

$$k(E) = \omega \left(\frac{E + E_0 - A_e}{E + E_0} \right)^{s-1}. \quad (9)$$

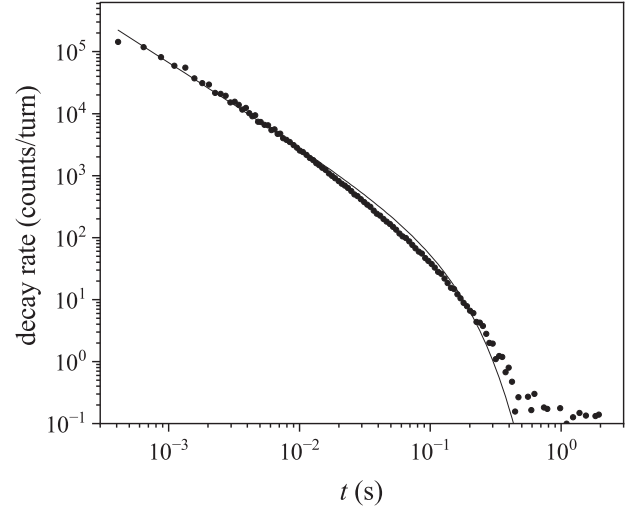


FIG. 9. Experimental decay rate (points) and the function fitted with Eq. (8) (line) for Au_7^- .

The energy E_0 is an offset in the caloric curve, and s is the canonical heat capacity in units of Boltzmann's constant. The value of E_0 does not enter the final result and is included only to give some generality to the expression. Assuming a frequency factor of 10^{14} s^{-1} for thermionic emission (thermal electron emission) and that the cluster is described by harmonic vibrations and given an electron affinity of 3.5 eV [12], we can calculate the missing term in Eq. (4) and express the emitted power by the measured time constant as

$$-\frac{dE}{dt} = \tau_2^{-1} \left(\frac{d \ln k}{dE} \right)^{-1} = 0.57 \text{ eV/s}. \quad (10)$$

The energy content differs from threshold energy for the process. This *kinetic shift* of 12% is included in the value given.

If the decay curve is to be represented by the small photon energy limit, the emitted photons must be smaller than the width of the energy distribution of the clusters that emit the electrons. Energy-resolved decay rates $r(E)$ occur in the general case according to

$$r(E) dE \propto e^{-k(E)t} k(E) dE. \quad (11)$$

This is a strongly peaked distribution as a function of energy. We can calculate an estimate of the width of the energy distribution by approximating the right-hand side of Eq. (11) with a Gaussian,

$$r(E) \propto \exp\left[-(E - \bar{E})^2 / \sigma_E^2\right]. \quad (12)$$

We estimate the standard deviation as

$$\sigma_E \approx \frac{\sqrt{2}}{s-1} A_e (\omega t)^{-1/(s-1)}. \quad (13)$$

This then gives, for the heptamer,

$$\sigma_E = 0.043 \text{ eV}. \quad (14)$$

Using that estimate for the highest possible photon energy for which the fit is applicable, $h\nu = 0.043$ eV, gives a photon emission rate constant of no less than $0.57/0.043 \text{ s}^{-1} = 13 \text{ s}^{-1}$. Although this lower limit for the emission constant

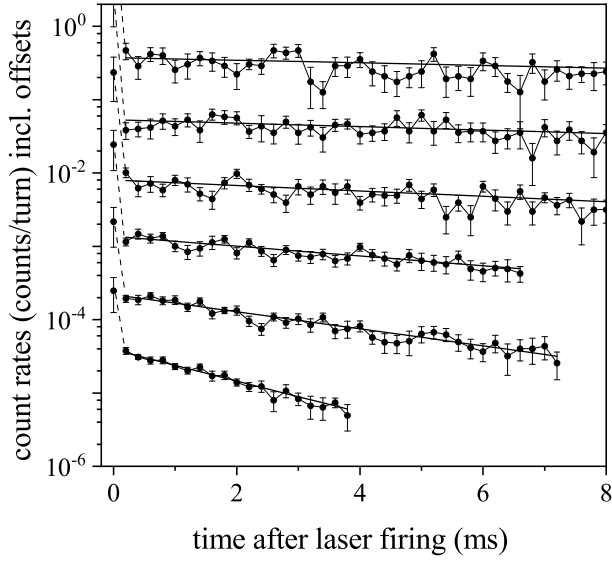


FIG. 10. The measured photoenhanced signal of Au_7^- , turn by turn after excitation. The curves (displaced on the ordinate with a constant factor between each) are recorded at laser firing times of, from bottom to top, 0.12 s, 0.22 s, etc., up to 0.62 s. Error bars are statistical. The curves for the laser firing times of 0.72, 0.82, and 0.92 s were similar but too flat to yield time constants.

is easy to fulfill for both types of cooling, vibrational and RF, it is consistent with vibrational cooling, and with the upper limit of the photon energy of 0.043 eV, it strongly suggests that the cooling is vibrational in the case of Au_7^- .

E. $N = 5$ photoexcitation

The photoinduced decay of Au_7^- was measured with 450-nm (2.76-eV) light from 0.12 to 0.92 s in steps of 100 ms. The decays were measured on timescales from 100 μs to several milliseconds after laser excitation. The energies sampled are therefore 2.76 eV below the energy corresponding to decay time constants on the few-hundred-microsecond timescale.

In Fig. 10 we show the decays as a function of time for each turn in the ring after the laser pulse for different laser firing times between 0.12 and 0.62 s. Excluding the first peaks, the decays are very well represented by single exponentials. The first peak is dominated by fast decays caused by the absorption of two or more photons. The decays during the following turns in the ring must be single-photon absorption to be consistent with single-exponential decay. (A mixture of single- and double-photon decays will give curves composed of at least two exponentials.) The fitted photon emission time constants are shown in Fig. 11 vs the laser firing time. There is a clear and smooth decrease of the time constants with laser firing time, corresponding to a rate constant that varies as $k(t) = 925 \text{ s}^{-1} \exp(-4.96 \text{ s}^{-1} t)$. The total integrated intensities of the six spectra are identical within the uncertainties. The integrated intensity of the observed part of the distribution is therefore constant.

The exponential decay indicates that the decaying clusters are sampled from a strongly peaked part of the energy distribution, rather than from a flat energy distribution. To observe

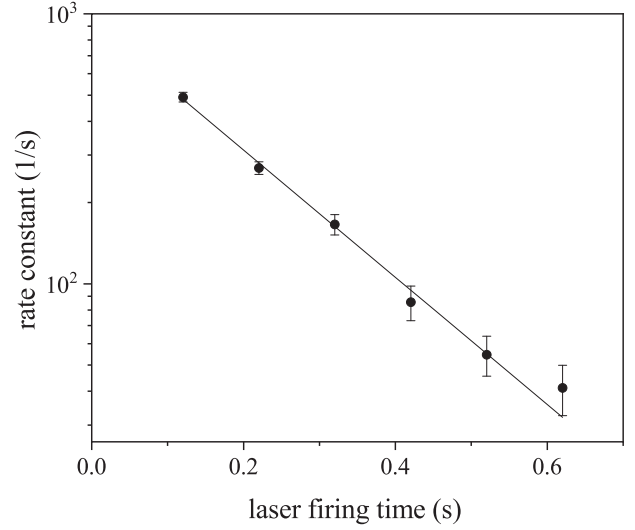


FIG. 11. The fitted rate constants for the time decay of the photon-enhanced electron emission signals for Au_7^- shown in Fig. 10. Error bars are calculated by error propagation. The fitted straight line has a slope of 4.96 s^{-1} .

single-exponential decay for the total decay rate, the energy distribution should be narrower than the function

$$r(E) = k(E)e^{-k(E)t}, \quad (15)$$

similar to the condition in Eq. (11) to distinguish small and large photon energy scenarios. The expression for this width is calculated in Eq. (13). With $A_e = 3.0 \text{ eV}$ [12], values of $s = 3N - 6$ valid for harmonic oscillators of an $N = 5$ cluster, and frequency factor $\omega = 10^{14} \text{ s}^{-1}$, the value is

$$\sigma_E = 0.045 \text{ eV}. \quad (16)$$

The timescale t used in Eq. (13) is the one for the measurement of the decay curves, which will summarily be set to 1 ms.

The energy emission rate reflected in the decrease of the emission rate constant with time is calculated with the relation

$$-4.96 \text{ s}^{-1} = \frac{dE}{dt} \frac{d \ln k}{dE}. \quad (17)$$

A little algebra and setting the kinetic shift to zero, $E + E_0 \approx A_e$, give

$$-\frac{dE}{dt} = \frac{4.96}{s-1} \frac{A_e}{(\omega t)^{1/(s-1)}} \text{ s}^{-1} = 0.033 \text{ eV/s}. \quad (18)$$

This is an average value over the measured time, as it is based on the average logarithmic slope of the fitted rate constant (see Fig. 11).

The small observed rate constant indicates that the energy is emitted in vibrational transitions. This is also consistent with the observation of purely exponential decay rates fitted at all six laser firing times. Larger photon energies would induce either loss of intensity, which is not seen, as mentioned, or deviations from exponential decays, which is also not seen. In contrast to electronic transitions, vibrational transitions have a weak internal energy dependence. As shown in Ref. [33], this feature conserves the shape of energy distributions in an ensemble when it cools by emission of IR photons, apart from

a scale factor, except at the lowest excitation energies. Hence, for such cases no width develops on the energy distribution with time, and the decay remains exponential, as observed.

IV. SUMMARY AND CONCLUSIONS

The spontaneous decays of anionic gold clusters were measured in the DESIREE storage ring. The results showed strong similarities to the two other coinage metals, copper [16] and silver [17], in particular for the decay of the dimer, which was investigated with respect to the branching between electron and atom emission.

The radiative cooling times display a strong odd-even effect for clusters $N = 6-13$, similar to the behavior previously seen for the gold cationic clusters [7] but with the striking difference that anionic odd- N clusters cool *slower* than even- N clusters, in a reversal of the oscillation pattern seen for the cations. Furthermore, time constants are 3 to 4 orders longer for anions, but the relative oscillation amplitude is quite similar for the two charge states. The fit of the decay curve of the heptamer indicates vibrational radiative cooling in this case. The precise reason for the very strong odd-even oscillations with size for gold clusters is still somewhat unclear. Photoexcitation experiments on the pentamer showed that this cluster size had cooled to a very low and well-defined internal energy already after 0.12 s, making the decays exponential. The decay constants were also found to vary exponentially with laser firing time, yielding an energy loss rate of 0.033 eV/s and a time constant of 0.20 s, indicating vibrational cooling also in this case.

In summary, the answers to the questions asked in the Introduction, whether the gold cluster anions will show RF and, if they do, whether they will show the same odd-even systematics as the cations, are probably not and definitely not, respectively. The reason that the first conclusion comes with a qualifier is that the strong indication of vibrational cooling is derived from the late photoexcitation experiments on cooled clusters vs the odd-even effect measured on the spontaneously decaying and therefore hotter clusters.

The other two questions both have clearer answers. Yes, the behavior which we tentatively ascribe to the presence of both high and low angular momenta is seen in the decay curves for the small clusters. The gold dimer anion indeed shows a clear signature of breakdown of the Born-Oppenheimer separation, in close analogy to the silver and copper dimer anions.

ACKNOWLEDGMENTS

This work was performed at the Swedish National Research Infrastructure, DESIREE (Swedish Research Council Contracts No. 2017-00621 and No. 2021-00155). It was supported with a beam time grant to K.H. H.C., H.Z., and H.T.S. thank the Swedish Research Council for individual project grants (with Contracts No. 2023-03833, No. 2020-03437, and No. 2022-02822) and acknowledge the project grant ‘‘Probing charge- and mass- transfer reactions on the atomic level’’ (2018.0028) from the Knut and Alice Wallenberg Foundation. This publication is based upon work from COST Action CA18212 - Molecular Dynamics in the GAS phase

(MD-GAS), supported by COST (European Cooperation in Science and Technology).

APPENDIX

The fit of the spontaneous decay rates with power laws requires that the time of creation of the clusters is known precisely. In this Appendix we calculate the time offset and show that the value is close to zero with the preset electronic timing.

The counts in a single turn in the ring arise from ions that have been generated at different times in the source but stored equally long in the ring, modulo the spread in the decay position and the very small difference in the speed of the neutral detected. The two spreads are so small that we can assign a single time to all decays that occur and are detected in any specific turn in the ring. The binning of multiple turns improves statistics and has the added advantage that it tends to average out the already small but nonstatistical betatron oscillations and related oscillations in the recorded neutralization yields that appear due to variations in detection efficiencies [34].

The measured time of decay potentially differs from the time elapsed since the creation of the clusters in the source, as the acquisition timer is started during ion transit through the mass-selection trajectory. The time of detection refers to the neutral particle produced in a decay in the straight section of the ring on the detector side of the ring. Relative to the detection time, the decay time is earlier by the amount of time it takes to move from the decay position to the detector t_{dt} . It is

$$t_{dt} = 1.7m\sqrt{N}/v_1, \quad (\text{A1})$$

where the length is the flight distance between the decay and detector and v_1 is the speed of the monomer at the acceleration energy used for this mass.

We denote the number of turns in the ring before detection by n , starting the count with $n = 1$ at the first half-turn detection, corresponding to labeling the first peak seen in the spectrum as 1. The time from production to detection of a decay during turn number n is then given by t_{dt} , an electronic offset t_{el} , which includes both the operation time of the detector and a delay in acquisition electronics, the circulation time t_{ci} , and the time from creation in the source to the arrival at the decay position in the first turn t_s . For the detection time of peak n the time is

$$t_{N,n} = t_{el} + t_s + (n - 1)t_{ci} + t_{dt}. \quad (\text{A2})$$

The first term is cluster size independent. The other three terms are proportional to \sqrt{N} , up to the two acceleration voltages used. In terms of the length of the ring ℓ and the source-to-decay point length ℓ_s , the peak times are, with $v_N = v_1/\sqrt{N}$,

$$t_{N,n} = t_{el} + \ell_s/v_N + (n - 1)\ell/v_N + 1.7m/v_N. \quad (\text{A3})$$

The time-resolved peaks for a given size allow us to plot t_N vs n to find the parameter $\ell\sqrt{N}/v_1$ and the intercept given by $t_{el} + \ell_s\sqrt{N}/v_1 + 1.7m\sqrt{N}/v_1$. Once these intercepts are determined, they are plotted vs \sqrt{N} , from which we get the value for $\ell_s/v_1 = 65.1\mu\text{s}$ from the slope. The electronic offset t_{el} was found to be less than $1\mu\text{s}$, much smaller than the flight

time of the first detected peak, and can be ignored. The value of ℓ/v_1 was found to be 86.9 μs for an acceleration energy of 10 keV. The analysis then gives the true decay times in terms

of the measured peak positions as

$$t_{N,\text{true}} = t_N - 1.7 \text{ m}\sqrt{N}/v_1. \quad (\text{A4})$$

-
- [1] I. Katakuse, T. Ichihara, Y. Fujita, T. Matsuo, T. Sakurai, and H. Matsuda, *Int. J. Mass Spectrom. Ion Processes* **67**, 229 (1985).
- [2] I. Katakuse, T. Ichihara, Y. Fujita, T. Matsuo, T. Sakurai, and H. Matsuda, *Int. J. Mass Spectrom. Ion Processes* **74**, 33 (1986).
- [3] K. Hansen, *Chem. Phys.* **530**, 110637 (2020).
- [4] A. Nitzan and J. Jortner, *J. Chem. Phys.* **71**, 3524 (1979).
- [5] S. Leach, in *Polycyclic Aromatic Hydrocarbons and Astrophysics*, edited by A. Léger, L. d’Hendecourt, and N. Boccarda, NATO ASI Series, Series C: Mathematical and Physical Sciences (Reidel, Dordrecht, 1987), Vol. 191, pp. 99–127.
- [6] A. Léger, P. Boissel, and L. d’Hendecourt, *Phys. Rev. Lett.* **60**, 921 (1988).
- [7] K. Hansen, P. Ferrari, E. Janssens, and P. Lievens, *Phys. Rev. A* **96**, 022511 (2017).
- [8] A. E. Green, A. S. Gentleman, W. Schöllkopf, A. Fielicke, and S. R. Mackenzie, *Phys. Rev. Lett.* **127**, 033002 (2021).
- [9] K. Hansen, P. F. Ramirez, E. Janssens, and P. Lievens, *J. Phys. Chem. C* **121**, 10663 (2017).
- [10] C. Jackschath, I. Rabin, and W. Schulze, *Ber. Bunsenges. Phys. Chem* **96**, 1200 (1992).
- [11] J. Ho, K. M. Ervin, and W. C. Lineberger, *J. Chem. Phys.* **93**, 6987 (1990).
- [12] K. J. Taylor, C. L. Pettiette-Hall, O. Cheshnovsky, and R. E. Smalley, *J. Chem. Phys.* **96**, 3319 (1992).
- [13] H. Häkkinen, B. Yoon, U. Landman, X. Li, H.-J. Zhai, and L.-S. Wang, *J. Phys. Chem. A* **107**, 6168 (2003).
- [14] M. Vogel, K. Hansen, A. Herlert, and L. Schweikhard, *Phys. Rev. Lett.* **87**, 013401 (2001).
- [15] K. Hansen, A. Herlert, L. Schweikhard, and M. Vogel, *Phys. Rev. A* **73**, 063202 (2006).
- [16] K. Hansen *et al.*, *Phys. Rev. A* **95**, 022511 (2017).
- [17] E. K. Anderson, M. Kamińska, K. C. Chartkunchand, G. Eklund, M. Gatchell, K. Hansen, H. Zettergren, H. Cederquist, and H. T. Schmidt, *Phys. Rev. A* **98**, 022705 (2018).
- [18] E. K. Anderson *et al.*, *Phys. Rev. Lett.* **124**, 173001 (2020).
- [19] E. K. Anderson *et al.*, *Phys. Rev. A* **107**, 062824 (2023).
- [20] R. D. Thomas *et al.*, *Rev. Sci. Instrum.* **82**, 065112 (2011).
- [21] H. T. Schmidt *et al.*, *Rev. Sci. Instrum.* **84**, 055115 (2013).
- [22] K. J. Taylor, C. Jin, J. Conceicao, L. Wang, O. Cheshnovsky, B. R. Johnson, P. J. Nordlander, and R. E. Smalley, *J. Chem. Phys.* **93**, 7515 (1990).
- [23] E. Bäckström *et al.*, *Phys. Rev. Lett.* **114**, 143003 (2015).
- [24] K. Hansen, J. U. Andersen, P. Hvelplund, S. P. Møller, U. V. Pedersen, and V. V. Petrunin, *Phys. Rev. Lett.* **87**, 123401 (2001).
- [25] J. Fedor, K. Hansen, J. U. Andersen, and P. Hvelplund, *Phys. Rev. Lett.* **94**, 113201 (2005).
- [26] S. Menk, S. Das, K. Blaum, M. W. Froese, M. Lange, M. Mukherjee, R. Repnow, D. Schwalm, R. von Hahn, and A. Wolf, *Phys. Rev. A* **89**, 022502 (2014).
- [27] P. Ferrari, E. Janssens, P. Lievens, and K. Hansen, *Int. Rev. Phys. Chem.* **38**, 405 (2019).
- [28] K. Hansen, *Statistical Physics of Nanoparticles in the Gas Phase*, Springer Series on Atomic, Optical, and Plasma Physics (Springer, Dordrecht, 2018), Vol. 73.
- [29] J. U. Andersen, E. Bonderup, and K. Hansen, *J. Chem. Phys.* **114**, 6518 (2001).
- [30] K. Hansen and E. E. B. Campbell, *J. Chem. Phys.* **104**, 5012 (1996).
- [31] J. U. Andersen, C. Brink, P. Hvelplund, M. O. Larsson, B. B. Nielsen, and H. Shen, *Phys. Rev. Lett.* **77**, 3991 (1996).
- [32] K. Hansen, *Phys. Rev. A* **102**, 052823 (2020).
- [33] K. Hansen, O. Licht, A. Kurbanov, and Y. Toker, *J. Phys. Chem. A* **127**, 2889 (2023).
- [34] R. Miyamoto, S. E. Kopp, A. Jansson, and M. J. Syphers, *Phys. Rev. Spec. Top. Accel. Beams* **11**, 084002 (2008).